water

Article

Improvement in Operation Efficiency of Shallow Geothermal Energy System—A Case Study in Shandong Province, China

Qinghua Wu [1,2,*], Yue Fan [1,2] and Xiao Wang [1,2]

[1] Changjiang River Scientific Research Institute, Wuhan 430010, China
[2] Key Laboratory of Geotechnical Mechanics and Engineering of Ministry of Water Resources, Wuhan 430010, China
* Correspondence: wqh0505@126.com

Abstract: Shallow geothermal energy (SGE) is a renewable energy source that has the advantage of being low-cost, clean, and locally sourced compared to fossil fuels, and is thus significant for China to achieve its future goals of carbon peaking and carbon neutrality. However, determining how to improve the operational efficiency of SGE systems is a key factor in the sustainable development and utilization of geothermal energy. This study examined the long-term operational efficiency of SGE systems and applied numerical simulation methods of hydro-thermal coupling to a SGE utilization project in Shandong Province, China. The effect of the distribution of pumping and injection wells on the operation efficiency of the SGE system was analyzed, and the parameter of operation efficiency, defined by the ratio of the practical minable shallow geothermal energy to the theoretical shallow geothermal energy, was applied to quantify the operation efficiency of the SGE system. The simulated results show that the phenomenon of heat transfixion is significant in the current operation scheme, where one of three pumping wells is located downstream of the study area, which indicates that the local groundwater flow field mainly controls the operation efficiency of the SGE system. In the optimized operation scheme, the distribution of pumping and injection wells can be adjusted according to the feature of groundwater flow and temperature fields. The degree of heat transfixion significantly declines and the operation efficiency increases by 71.5%. In addition, further improvements in the operational efficiency of the SGE system can be considered through the running time. The findings of this paper will be useful for the construction and management of SGE systems.

Keywords: groundwater; shallow geothermal energy; water source heat pump; heat transfixion; operation efficiency; numerical simulation

check for updates

Citation: Wu, Q.; Fan, Y.; Wang, X. Improvement in Operation Efficiency of Shallow Geothermal Energy System—A Case Study in Shandong Province, China. *Water* **2023**, *15*, 1409. https://doi.org/10.3390/w15071409

Academic Editor: Aldo Fiori

Received: 29 January 2023
Revised: 23 March 2023
Accepted: 25 March 2023
Published: 5 April 2023

1. Introduction

Shallow geothermal energy (SGE) is geothermal energy from 200 m below the Earth's surface. The SGE system can provide clean, secure, abundant, and economical energy [1], and is thus vital to reducing carbon dioxide emissions. Carbon dioxide is a major cause of global warming and the Paris Agreement on Climate Change (2015) recommended that all countries should reduce carbon dioxide emissions, mainly from fossil fuels, to limit global temperature rise to 1.5 °C above pre-industrial levels. Therefore, the Chinese government plans to reach peak carbon dioxide emissions by 2030 and be carbon neutral by 2060 [2]. One of the effective ways to achieve the above goal is to vigorously develop SGE. SGE could make a significant contribution to reducing CO_2 emissions and the gradual replacement of fossil fuels, while ensuring sustainable socio-economic development.

SGE is used in many countries, with a rising number of installations in recent decades; SGE systems have been developed and utilized in 40 countries [3]. SGE accounts for 59.2% of direct-use geothermal energy consumption per year in the world, and the total installed capacity and energy production are 77,547 MWt and 599,981 TJ, respectively [4]. According to a report by the International Energy Agency (IEA, 2021), the number of heat pumps has grown 10% per year in the last 5 years, and by 2050, geothermal energy production will reach about 100~210 TWh/y [5]. About 7000 TWh/y of SGE could be utilized in 31 provinces of China, reducing the emissions by 6.1 $\times$ 10^8 t/y CO_2, 1.98 $\times$ 10^6 t/y SO_2, and 6.1 $\times$ 10^8 t/y nitride [6]. SGE of heating/cooling systems has a coefficient of performance higher than 1, specifically between 3 to 7. This shows that the SGE system can produce more clean energy by consuming little electricity, thus reducing CO_2 emissions indirectly [7], although the initial construction cost of the SGE system is higher than that of the traditional heat-exchanging system [8].

Determining how to improve the operational efficiency of SGE systems is vital to the sustainable utilization of geothermal energy. The focus of researchers and engineers examining the sustainability of SGE systems is on system thermodynamics and the optimization of installation and operation stages, which can affect the energy exchange efficiency of SGE systems during the operation period. Andrea Aquino et al. showed that the factors affecting the sustainability of SGE systems were mainly the climate and ground properties, the installation operations, and the maintenance of the refrigerant circuit and the serviced building, and the optimization of installation and operation stages can improve the SGE system [9]. Furthermore, the efficiency of the SGE system can be mainly controlled by the quality and quantity of the groundwater, the choice of aquifers and filter pipes, the distance between hot and cold wells, and the location of wells [10]. Chang and Kin [11] confirmed that the thermal conductivity of the vertical closed U-loop ground heat exchanger increases with the increase in the larger diameter of the tube. A new innovative borehole heat exchanger structure comprising one outlet and three inlet pipes was proposed, and the experimental results showed that the average circulating water temperature of the structure was 1 and 3.7 °C lower than that of the traditional single-U and double-U systems, respectively [12]. The thermal conductivity of materials transferring the heat from the pipe and the earth was analyzed, and results showed that the temperature increase on the borehole wall of the inclined pipe could be 10–35% lower than that of the vertical pipe, showing that the structure can affect the SGE system's long-term performance [13]. The installation costs were evaluated by the validated capacitance–resistance numerical model, considering the factors of the borehole diameter of the helical coil, the depth of the helical coil, and the spacing [14]. The parameter of COP was optimized using a methodology that operated on both heating and cooling models, and the maximum COP values for only heating and cooling operations were 4.25 and 3.32, respectively [15]. The method of life cycle assessment (LCA) was applied to assess the impact of the SGE system on the environment, mainly with respect to manufacturing, transportation, operation, energy consumption, and air emissions to the environmental system [16].

In particular, the operation efficiency of the SGE system is affected by heat transfixion from the groundwater between injection wells and pumping wells [17]. Regional hydrogeological conditions, the spatial distribution, and the operation scheme of pumping/injection wells have a significant impact on the phenomenon of heat transfixion [18]. However, determining how to improve the operation efficiency based on the design of pumping and injected wells, and how to quantify the operation efficiency of the SGE system during the cooling and heating period, has not been reported.

Therefore, an example of the SGE system was analyzed using the hydro-thermal coupling simulated mode in Shandong province of China. In this study, the groundwater flow and temperature fields with different spatial distributions and the operation schemes of pumping/injection wells were studied to assess the phenomenon of heat transfixion, and to propose optional operations for the SGE system. Firstly, the meteorology, hydrology, hydrogeology, and operation of the SGE system are introduced. Secondly, the mathematical model containing the groundwater flow and thermal transport codes, and the simulation scheme, are shown. Then, the simulation results of the current operation scheme and the improved operation scheme are analyzed. Lastly, the degree of heat transfixion and the accumulated minable shallow geothermal energy are discussed, and the main conclusions are presented, which may be valuable for SGE system operations.

2. Study Area

2.1. Meteorology and Hydrology

The SGE system was installed in 2017, in Zibo city, Shandong Province, China. The study area has a length and width of 1000 m, and is located in the flat topography of the Piedmont plain area. The SGE system is located in the center of the study area (Figure 1). The annual rainfall is 608 mm, concentrated from June to September. The annual average temperature is 12.2 °C, and the highest value of 26.2 °C and the lowest value of −3.8 °C occur in July and January, respectively. In addition, the nearest surface water is Taigong Lake, about 7.5 km away, which will not be affected by the long-term operation of the SGE system.

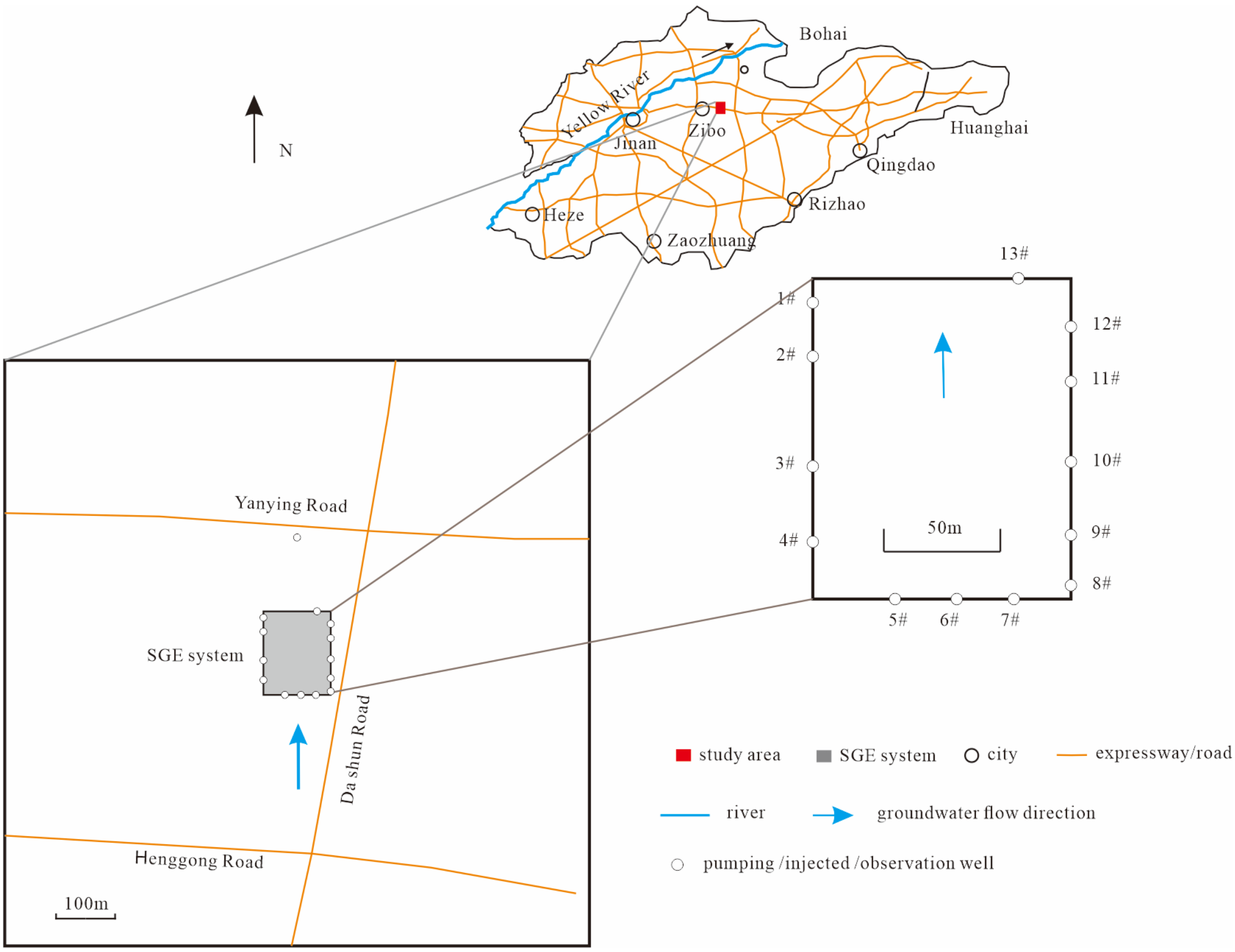

Figure 1. Study area and SGE system.

2.2. Hydrogeology

The study area is located in an alluvial-proluvial fan where the main lithologies of the confined aquifer are sand gravel and cobble gravel. The thickness of the aquifer is generally 50–100 m in the south, 150–200 m in the middle, and 300–350 m in the north. The water yields of single wells in cobble gravel and sand gravel aquifers are over 5000 and 1000–5000 m^3/d, respectively. The groundwater flows from south to north, i.e., from the mountain to the plain. The rainfall is the main recharge, followed by river seepage recharge and irrigation recharge. Local groundwater is mainly used for agricultural irrigation and centralized urban water supply. The hydro-chemical types of groundwater are HCO_3-Ca and HCO_3-Ca·Mg, with a degree of mineralization of 297–368 mg/L and a pH of 7.4–8.0.

2.3. Operation of the Shallow Geothermal Energy System

The SGE system in the study area could provide energy for an office building and hotel in summer and winter, with a heating and cooling area of 19,652.73 m^2. The cooling operation period of the SGE system is from June to September (summer), for a total of 120 days, while the heating operation period is from November to March (winter), for a total of 120 days, and the system will shut down at other times. At present, the SGE system involves three pumping wells (1#, 4#, and 8#) and ten injection wells, shown in Figure 1, with a 100% recharge rate. The difference between the groundwater and SGE system temperature is designed to be 5 °C, while the average temperature of the regional groundwater is 21 °C. Thus, without considering interannual fluctuations, the temperature of the pumping wells is a constant value of 21 °C, while the temperatures of the injection wells during the cooling and heating periods are 26 and 16 °C, respectively. The flux of each pumping well is 1512 m^3/d, and that for each injection well is 453.6 m^3/d. Observation wells, named obs1#, obs2#, etc., were installed in each well, and observation well obs14# was added 250 m from the northern boundary of the SGE system, as shown in Figure 1.

3. Methods

3.1. Conceptual Model of Hydrogeology

According to the borehole profile, the formation lithology is mainly clay, gravel, and limestone (Figure 2). The aquifer is confined with a depth of 45.8 m. The main water-bearing medium is gravel and is generalized to be an isotropic aquifer. The pumping and injection wells are completely penetrated wells.

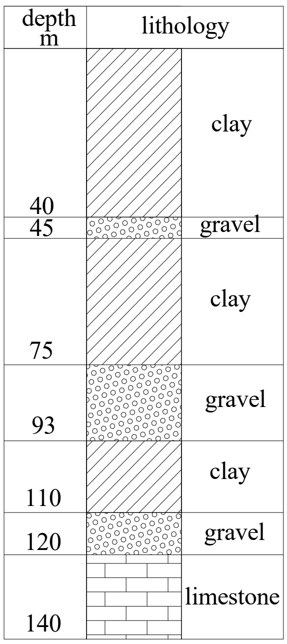

Figure 2. The profile of the borehole.

The groundwater flows from the south to the north, i.e., from the 4# well to the 1# well. Based on the pumping test, the range of influence for the pumping well is less than 81.5 m; therefore, the range of the conceptual model is suggested to be a size of 1000 m (length) × 1000 m (width) × 140 m (depth). The SGE system is located in the center of the square. The distance between the boundary and the SGE system is 500 m, and is not affected by the pumping wells. The south and north boundaries are considered as being constant head boundaries with head values of 29.74 and 28.09 m, respectively. The east and west boundaries are considered to be impermeable boundaries. The effect of rainfall is ignored in this simulation because of the impermeable pavement. During the operation period, the fluxes of the pumping and injection wells are constant.

For the thermal model, the upstream boundary is set to a constant temperature of 21 °C, and the other boundary conditions are considered to be heat exchange boundaries. The temperatures of the pumping wells are constant at 21 °C, while the temperatures of the injection wells during the cooling and heating periods are constant at 26 and 16 °C, respectively.

3.2. Mathematical Model

To analyze the operation efficiency of the SGE system under different schemes, the mathematical models of groundwater flow and heat transport were coupled and successfully simulated [19–21].

3.2.1. Mathematical Model of Groundwater Flow

The three-dimensional unsteady flow mathematical model is shown as follows:

$$\begin{cases} \frac{\partial}{\partial x_i}\left(K_{i,j}\frac{\partial H}{\partial x_j}\right)+\omega=S_s\frac{\partial H}{\partial t} \quad i,j=1,2,3 \\ H(x,y,z,t)|_{t_0}=H_0(x,y,z) \quad (x,y,z)\in\Omega \\ H(x,y,z,t)|_{\Gamma_1}=H(x,y,z,t) \quad (x,y,z)\in\Gamma_1 \\ K_{i,j}\frac{\partial H}{\partial n}\Big|_{\Gamma_2}=q(x,y,z,t) \quad (x,y,z)\in\Gamma_2 \end{cases} \tag{1}$$

where $K_{i,j}$ represents the hydraulic conductivities of the aquifer (LT^{-1}), H is the head of groundwater (L), ω is the source and sink term (T^{-1}), S_s is the specific storage (L^{-1}), t_0 is the initial time (T), H_0 is the water head at the initial time (L), q is recharge per unit area on the flux boundary ($L^2\ T^{-1}$), Γ_1 and Γ_2 are head boundary and flux boundary, respectively, and Ω is the computational domain.

3.2.2. Mathematical Model of Thermal Transport

The three-dimensional unsteady flow equation is shown as follows:

$$\begin{cases} \left\{\frac{\partial}{\partial x_i}\left(D_{i,j}\frac{\partial T}{\partial x_j}\right)-\frac{\partial}{\partial_{x_i}}(v_i\rho_w C_w T)+Q_T=[\theta\rho_w C_w+(1-\theta)\rho_s C_s]\frac{\partial T}{\partial t} \quad i,j=1,2,3 \right. \\ T(x,y,z,t_0)|_{\Omega}=T_0(x,y,z) \quad (x,y,z)\in\Omega \\ T(x,y,z,t)|_{\Gamma_1}=T(x,y,z,t) \quad (x,y,z)\in\Gamma_1 \\ T(x,y,z,t)|_{\Gamma_{wi}}=T_{wi}(z,t) \quad (x,y,z)\in\Gamma_w \end{cases} \tag{2}$$

where T is the temperature of the groundwater (Θ), $D_{i,j}$ is the hydrodynamic dispersion coefficient (L), v is the seepage velocity (LT-1), ρ_w is the density of groundwater (ML^{-3}), C_w and C_s are the thermal capacity of groundwater and soil ($L^2T^{-2}\Theta^{-1}$), respectively, t is the time (T), Γ_1 is temperature boundary and flux boundary, Q_T is the heat source and sink ($M^2\ MT^{-2}$), Γ_W is the injection and pumping wells, T_w is the temperature of the well (Θ).

The heat exchange between groundwater and aquifer media is assumed to occur instantaneously in the model, ignoring the hysteresis of heat exchange.

The lower interface of the limestone layer is set to relative zero elevation, i.e., $z = 0$ m, and is upwards positive; the origin of the coordinate system is set in the southwest corner of the study area, i.e., the value of x increases from west to east, while the value of y increases from south to north. The mathematical model is discretized using the finite element method.

3.2.3. Model Condition Setting

Grid dissection was performed using the Grid Builder program, and the subsurface water flow and heat transport model were solved by the finite element calculation software Feflow, which can simulate flow-, mass-, and heat-transport processes in porous media. According to the conceptual model, the model was divided into 6 vertical layers, and the finite element mesh generation of the model followed the rule that the size of the mesh is 1 m × 1 m in the region and 0.2 m × 0.2 m for the wells. The geometric model of the model is shown in Figure 3.

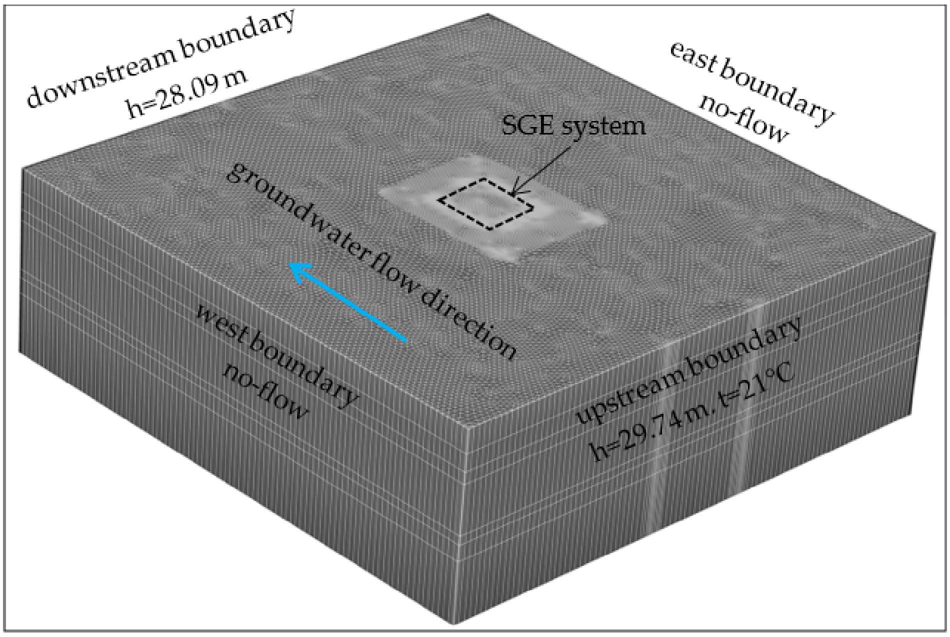

Figure 3. The geometric model of the model.

(1) Boundary condition

For the steady flow model, the water head at upstream and downstream boundaries is 29.74 and 28.09 m, respectively, and the west and east boundaries are no-flow boundaries, as shown in Formula (3). The flux of each pumping well is 1512 m^3/d, and 453.6 or 756 m^3/d for each injection well, according to Table 1.

Table 1. Simulation scheme.

Scheme	Pumping Well	Injection Well
F1	1#, 4#, and 8#, each well with the flux of 1512 m^3/d	other wells, each well with the recharge flux of 453.6 m^3/d
F2	In the cooling period, 4#, 6#, and 8# with the flux of 1512 m^3/d, while in the heating period, 1#, 6#, and 8# with the flux of 1512 m^3/d	In the cooling period, 1#, 2#, 10#, 11#, 12#, and 13# with the recharge flux of 756 m^3/d, while in the heating period, 3#, 4#, 8#, 9#, and 10# with the recharge flux of 756 m^3/d
F3	In the cooling period, 1#, 3#, and 5# with the flux of 1512 m^3/d, while in the heating period, 10#, 12#, and 13# with the flux of 1512 m^3/d	In the cooling period, 8#, 9#, 10#, 11#, 12#, and 13# with the recharge flux of 756 m^3/d, while in the heating period, 1#, 2#, 3#, 4#, 5#, and 6# with the recharge flux of 756 m^3/d

$$\begin{cases} H(x,y,z,t) = 29.74\text{m} & x \in [0,1000\text{m}],\ y = 0\text{m}, \quad z \in [0,140\text{m}] \\ H(x,y,z,t) = 28.90\text{m} & x \in [0,1000\text{m}],\ y = 1000\text{m}, z \in [0,140\text{m}] \\ K_{i,j}\frac{\partial H}{\partial n} = 0\text{m}^3/\text{d} & x = 0\text{m}, y \in [0,1000\text{m}], \quad z \in [0,140\text{m}] \\ K_{i,j}\frac{\partial H}{\partial n} = 0\text{m}^3/\text{d} & x = 1000\text{m}, y \in [0,1000\text{m}],\ z \in [0,140\text{m}] \\ K_{i,j}\frac{\partial H}{\partial n}\Big|_{\Gamma_2} = 1512\text{m}^3/\text{d} & \Gamma_2 \text{ is pumping wells} \\ K_{i,j}\frac{\partial H}{\partial n}\Big|_{\Gamma_2} = 453.6\text{or}756\text{m}^3/\text{d} & \Gamma_2 \text{ is injection wells} \end{cases} \quad (3)$$

For the thermal transport model, the temperature at the upstream boundary is 21 °C, while the other boundaries have free heat exchange. During the cooling and heating operation periods, the temperatures of injection are 16 and 26 °C, respectively, as shown in Formula (4):

$$\begin{cases} T(x,y,z,t) = 21\ ^{\circ}\mathrm{C} & x \in [0, 1000\ \mathrm{m}], y = 0\ \mathrm{m}, z \in [0,\ 140\ \mathrm{m}] \\ T(x,y,z,t)|_{\Gamma_{wi}} = 16\ ^{\circ}\mathrm{C} & \Gamma_{wi} \text{ is inected wells for heating period} \\ T(x,y,z,t)|_{\Gamma_{wi}} = 26\ ^{\circ}\mathrm{C} & \Gamma_{wi} \text{ is inected wells for cooling period} \end{cases} \tag{4}$$

(2) Initial conditions

The water head of initial conditions for the unstable three-dimensional model is obtained from the stable three-dimensional model, which is the same as the unstable 3 D model expect for the wells. Whereas the initial temperature is set to 21 °C, the initial temperatures for cooling and heating periods are 26 and 16 °C, respectively, as shown in Formula (5):

$$\begin{cases} T(x,y,z,t_0)|_{\Gamma} = 21\ ^{\circ}\mathrm{C} & \Gamma \text{ is for inected wells during heating period} \\ T(x,y,z,t)|_{\Gamma_{wi}} = 26\ ^{\circ}\mathrm{C} & \Gamma_{wi} \text{ is for inected wells during cooling period} \\ T(x,y,z,t)|_{\Gamma_{wi}} = 16\ ^{\circ}\mathrm{C} & \Gamma_{wi} \text{ is for inected wells during heating period} \end{cases} \tag{5}$$

3.3. Simulation Scheme

The purpose of this study was to evaluate the operational efficiency of the SGE system and to analyze the optimal operational scheme based on a series of simulated schemes for comparison, as shown in Table 1.

The SGE system operates intermittently for 5 years with the scheme shown in Figure 4. In the first year, the cooling period is from June to September (model period of 0–120 days), while the heating period is November to March (model period of 170–289 days); the system does not operate during other periods. The spatial distribution pumping-injection wells, and the recharge of injection wells, are simulated to analyze the operation efficiency of the SGE system.

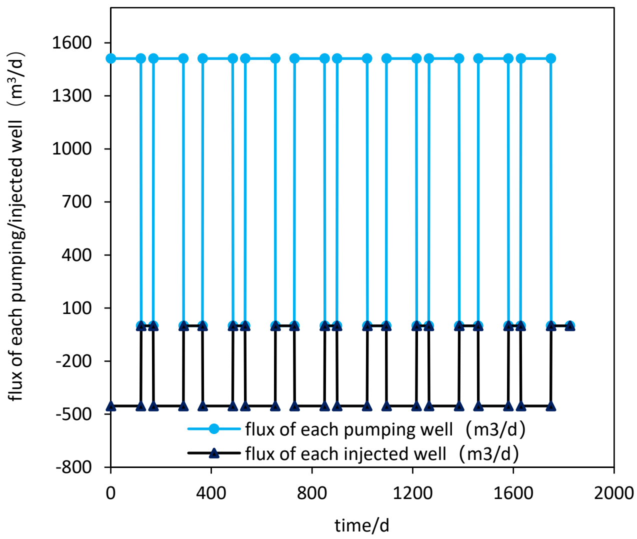

Figure 4. The flux of each pumping/injection well vs. time for the simulation schemes of the SGE system.

4. Results

4.1. Simulation of the Current Operation Scheme

4.1.1. Characteristics of Groundwater Flow

Since groundwater is a medium for transferring and exchanging heat, the flow characteristics of groundwater may significantly influence the SGE system operation. The characteristics of groundwater flow are controlled by the local groundwater and the operation of the SGE system resulting from the spatial distribution of pumping and recharge wells. Therefore, the SGE system layout and operating scheme may affect the operational efficiency. The simulation results of the current operation scheme (F1) show that the groundwater flow field reaches a steady state in 1 day after the system operation, and no obvious change in groundwater level is observed near the boundary, which implies that the impact of the SGE system on the groundwater flow field is minimal.

4.1.2. Characteristics of Thermal Transport

During the operation of the SGE system, the heat transfixion phenomenon can be analyzed by observing the temperature of the pumping wells. Figures 5 and 6 show that thermal transfixion is observed in all pumping wells.

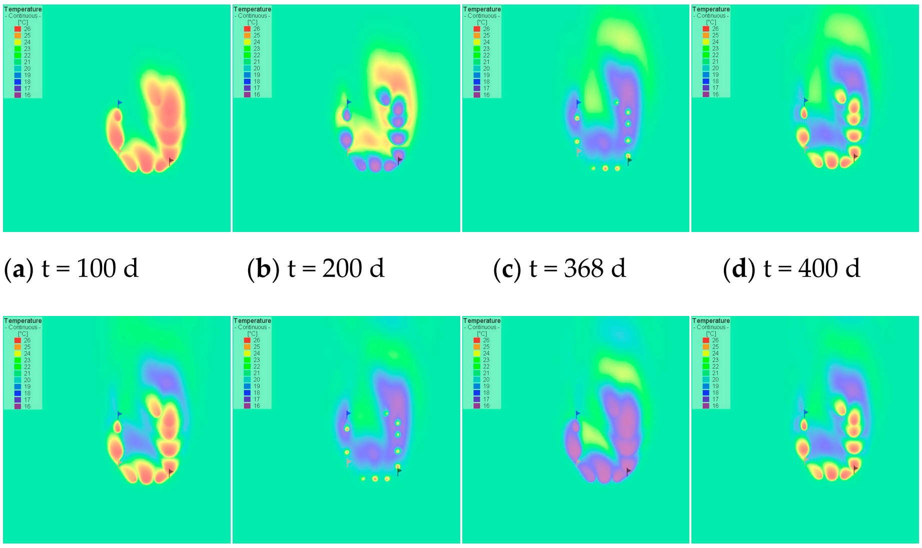

(**a**) t = 100 d (**b**) t = 200 d (**c**) t = 368 d (**d**) t = 400 d

(**e**) t = 800 d (**f**) t = 1098 d (**g**) t = 1375 d (**h**) t = 1500 d

Figure 5. Temperature distributions of main model area in five cooling and heating periods. Note: (**a**,**c**,**e**,**g**) were in the cooling period, while (**b**,**d**,**f**,**h**) were in the heating period.

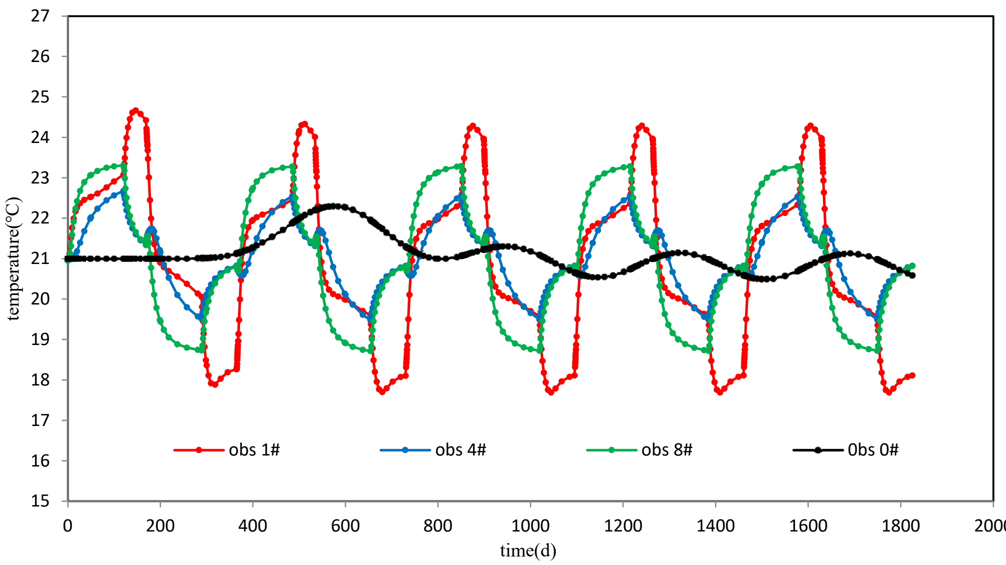

Figure 6. Temperature vs. time for observation wells (F1).

The groundwater with high temperature injected from injection well 2# first reaches pumping well 1# within 3.7 days. The temperature of well 1# rapidly increases to 22.4 °C and then gradually increases in a linear fashion to 23.1 °C until the SGE system stops within 120 days. However, the temperature of pumping well #1 rises more rapidly in 157 days, reaching 24.6 °C (the highest value), which implies that shutting down the pumping wells could reduce mixing of local groundwater with hot injected water. When the SGE system runs for heating from day 171 to day 289, the temperature of pumping well 1# decreases linearly to 21 °C for 190 days and then slowly decreases to 20 °C until the SGE system stops again. The different descent velocities indicate the mixing process of local groundwater and injected water with a lower temperature of 16 °C. As seen in Figure 4, the temperature characteristics of observation well 1# in the next four years are similar, which indicates that the influence of the SGE system on pumping well 1# reaches a new equilibrium after 365 days with the same annual characteristics.

The temperatures of pumping well 4# are influenced by the local groundwater, and injection wells 3# and 5#. The phenomenon of heat transfixion in pumping well 4# is monitored on day 20, later than for pumping well 1#. After day 20, the temperature of pumping well 4# increases rapidly to 22.7 °C (the highest value) until the SGE system stops on day 120. Then it drops to 21.4 °C until the SGE system stops on day 170. It increases slightly to 21.7 °C on day 182.7, and the temperature decreases continually to 19.5 °C until the heating program running on day 289. This indicates that the local groundwater has a more important influence on pumping well 4# than well 1#.

The temperature of pumping well 8# is influenced by the local groundwater, and injection wells 7# and 9#. The hot groundwater from the injection wells reaches pumping well 8# in 6.8 days. The characteristics of temperature and time are similar to those of pumping well 4#, but with a larger positive peak value of 23.3 °C on day 120 and a smaller positive peak value of 18.7 °C on day 289, which shows that the injection wells can have a more important influence on pumping well 8#.

The relationship between temperature and time of observation well 0#, which is located 250 m from the north boundary of the SGE system, reveals that the first injection hot groundwater during 0–120 days arrives at observation well 0# on day 365, and reaches the peak value of 22.3 °C on day 573.2. After day 1333.8, the influence of the SGE system on observation well 0# achieves balance.

4.1.3. Operation Efficiency Evaluation of the SGE System

The operation efficiency of the SGE system is mainly controlled by equipment characteristics, thermal loss of water delivery pipes, thermal conductivity of the groundwater and the soil layer, the hydraulic conductivity coefficient of the aquifer, and temperatures of the local groundwater and air. In this paper, the operation efficiency is defined by the formulas as follows:

$$\eta = \frac{\Delta E_{pr}}{\Delta E_{th}} \times 100\% \tag{6}$$

$$\Delta E_{pr} = \sum_{i=1}^{M}\sum_{j=1}^{N} \gamma C_w \rho_w Q_i t_{i,j} - t_{i,j-1})(\frac{T_{i,j} + T_{i,j-1}}{2} - T_{outlet}) \tag{7}$$

$$\Delta E_{th} = \gamma \cdot C_w \cdot \Delta T \cdot \Delta t \cdot \rho_w \sum_{i=1}^{M} Q_i \tag{8}$$

where η is the operation efficiency coefficient of the SGE system; ΔE_{pr} is the practical minable shallow geothermal energy, kwh; ΔE_{th} is the theoretical minable shallow geothermal energy, kwh; M is the number of the pumping well; N is the calculation number; Q_i is the flux of the i pumping well, m^3/d; C_w is the specific heat capacity, J/(kg·°C); ρ_w is the density of water, kg/m^3; $T_{i,j}$ and $T_{i,j-1}$ are the temperatures of the i pumping well for the time of $t_{i,j}$ and $t_{i,j-1}$, °C, respectively; T_{outlet} represents the temperatures of the outlet water, °C; γ is the energy exchange efficiency, related to the energy loss of the heat transfer system and the geothermal energy loss during the operation of the SGE system, generally with the value of

25% [22]; ΔT is the temperature difference between the groundwater and outlet water of the heat exchange equipment, °C; Δt is the operation time of the SGE system, day.

Based on the assumption that the temperature of the local groundwater is constant at 21.0 °C, and the temperatures of the outlet water of the SGE system are 16 and 26 °C in heating and cooling periods, respectively, the operation efficiency coefficient of the SGE system is mainly analyzed according to the temperature of the pumping wells, which can be influenced by both injection water and local groundwater.

The relationship between the operation efficiency coefficient η and time is shown in Figure 7, which indicates that the value of parameter η declines rapidly during the SGE system operation during the cooling or heating periods, because of heat transfixion. Significantly, the values of the initial operation efficiency coefficient are always larger than those of the previous cooling or heating periods, expect for the first cooling period; this shows that the injection groundwater, which has a higher temperature in the cooling period, reaches the pumping wells. After the cooling period, the SGE system is terminated for about 3 months, during which the temperature of the local groundwater rises continually. Thus, the temperatures of pumping wells 1#, 4#, and 8# are higher than the 21.5 °C of the local groundwater, at 24.2, 21.4, and 21.5 °C, respectively, at the beginning of the first heating period. In the heating period, the higher value of the operation efficiency coefficient is mainly because of the temperature of the pumping wells.

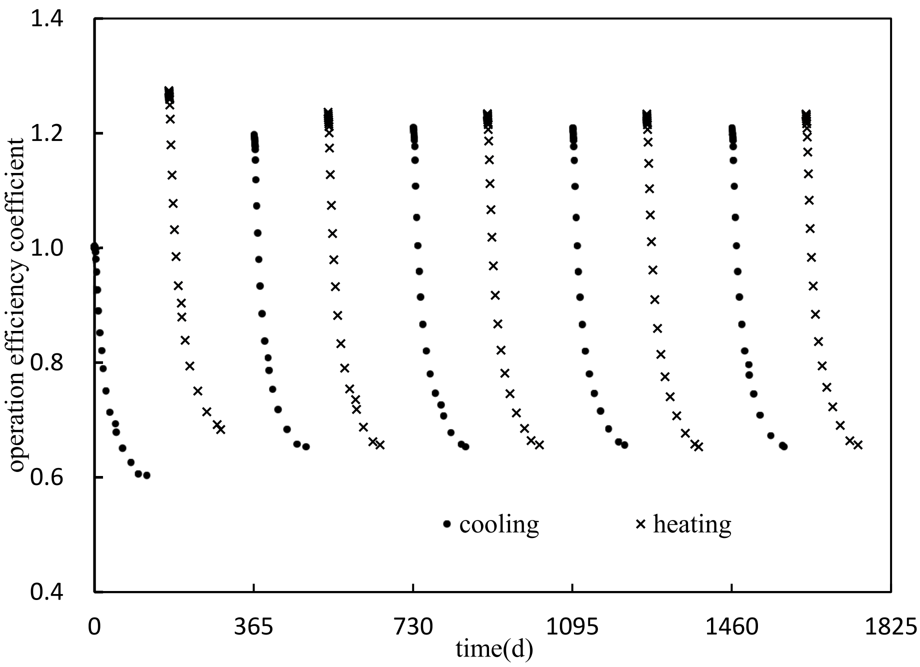

Figure 7. The relationship between operation efficiency coefficient η and time for the present operation (F1).

The temperature difference between the pumping well and local groundwater during the heating and cooling periods is greater, resulting in a higher operation efficiency coefficient. Consequently, there would be high operation efficiency of the SGE system without the influence of heat transfixion and, after the cooling period, the injection wells are all transferred to pumping wells, therefore obtaining a higher temperature for the heating period.

4.2. Simulation of the Optimized Operation Schemes

Based on the simulated result of the current operation scheme, the groundwater flow characteristics do not change significantly in both heating and cooling periods with the same pumping and injection flow rates. Therefore, the subsequent analysis focuses on evaluating the thermal transport characteristics and operational efficiency. According to the simulation results, the phenomenon of heat transfixion is significant, especially for pumping well 1#; as a result, the distance from upstream injection well 2# is only 23.5 m. Consequently, the operation efficiency of the SGE system could be promoted by changing the spatial distribution of the pumping and injection wells. For instance, during the cooling period, the groundwater at 21 °C is pumped into the SGE system and the temperature difference of about 5 °C is transferred into "cooling energy" in order to cool the building in summer, resulting in injection water with a higher temperature of 26 °C. Then, during the heating period, some injection wells are changed to pumping wells in order to obtain a higher temperature, thereby increasing the operation efficiency of the SGE system.

4.2.1. Characteristics of Thermal Transport for F2

There is difference between F1 and F2 in terms of the characteristic of thermal transport. The phenomenon of heat transfixion appeared again; however, the duration of thermal transfixion was significantly shorter and the extent was reduced.

During the first cooling period, wells 4#, 6#, and 8# are set as pumping wells, while wells 1#, 2#, 10#, 12#, and 13# are set as injection wells. The temperatures of pumping wells 4#, 6#, and 8# first rise to 21.1 °C on days 120, 90, and 38.2, respectively, resulting from the injection groundwater with a higher temperature. The temperature feature of well 8# is different from that of wells 4# and 6#, i.e., after the heat transfixion occurs, the temperature increases linearly to 21.9 °C on day 120.

During the first heating period, wells 1#, 6#, and 13# are set as pumping wells, while wells 3#, 4#, 8#, 9#, and 10# are set as injection wells. Due to the higher initial temperature, the temperatures of pumping wells 1# and 13# decrease to 20.7 °C on days 60 and 90 after heating, and finally reach 18.2 and 19.2 °C. The temperature of pumping well 6# decreases to 20.8 °C on day 30, and reaches 19.7 °C.

According to Figure 8, the trend of temperature vs. time is steady from the second year. At the beginning of the second cooling period, the temperatures of pumping wells 4# and 6#, are 20.2 and 20.9 °C, respectively, lower than the first cooling period, then the temperatures decrease slowly, which is different from the first year. The temperature reaches the lowest values of 20.1 and 20.5 °C after the second cooling, and then finally increase to 20.6 and 20.7 °C. The temperature of pumping well 8#, with an initial value of 20.0 °C, decreases continually from day 0 to day 20 after the second cooling, then increases linearly to the peak value of 21.6 °C, which is lower than that of the first cooling period. However, the temperature characteristics of pumping wells are similar to those of the first heating period.

4.2.2. Characteristics of Thermal Transport for F3

In order to reduce the influence of heat transfixion on the operation efficiency of the SGE system, the pumping wells and injection wells are installed in the west and east, respectively. The location of the pumping wells and injection wells are switched reciprocally in the cooling and heating periods. During the cooling period, wells 1#, 3#, and 5# are set as pumping wells, while wells 8#, 9#, 10#, 11#, 12#, and 13# are set as injection wells. During the heating period, wells 10#, 12#, and 13# are set as pumping wells, and wells 1#, 2#, 3#, 4#, 5#, and 6# are set as injection wells.

During the first cooling period, the three pumping wells have similar features. The temperatures of pumping wells 1#, 3#, and 5# rise to 21.1 °C on days 80, 80, and 60, respectively, because of the heat transfixion, and the temperatures of the pumping wells increase linearly to 22.0, 21.9, and 21.7 °C on day 120. The result is shown in Figure 9.

After the first cooling period, the thermal transport changes because of the local groundwater flow, causing the temperatures of the three pumping wells to go down continually. At the beginning of the first heating period, the temperatures of the three pumping wells, of 25.9, 25.9, and 25.8 °C, respectively, are higher than those of the schemes F1 and F2. Because of the local groundwater flow gradient and local groundwater thermal gradient, the temperatures of the pumping wells decrease continually. Significantly, the temperatures of pumping wells 10# and 12# decrease to less than 21 °C on days 70 and 110 after the first heating period, while the temperature of pumping well 13# is 21.8 °C on day 120, which shows that there might be a higher operation efficiency for the SGE system.

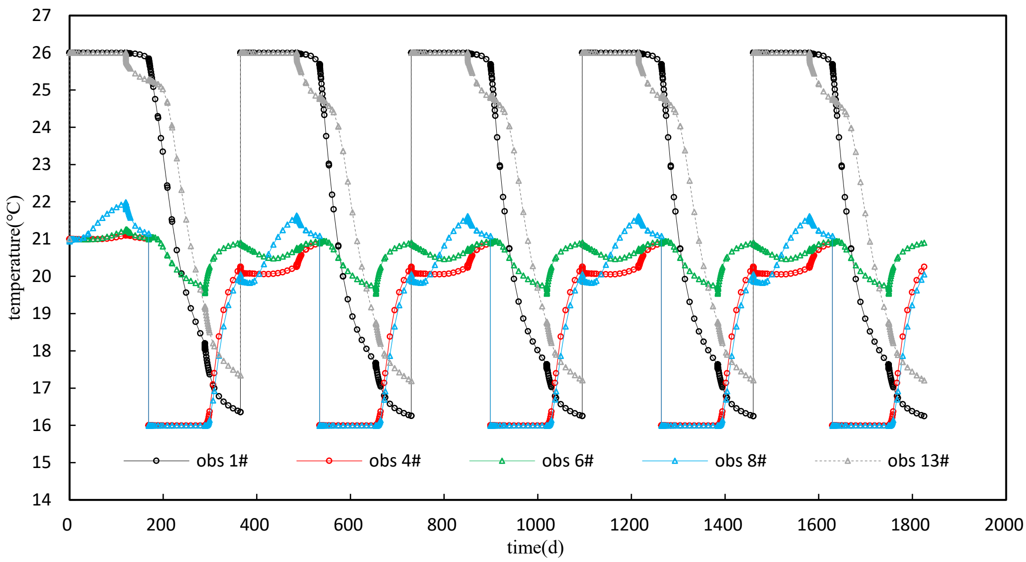

Figure 8. Temperature vs. time for observation wells (F2).

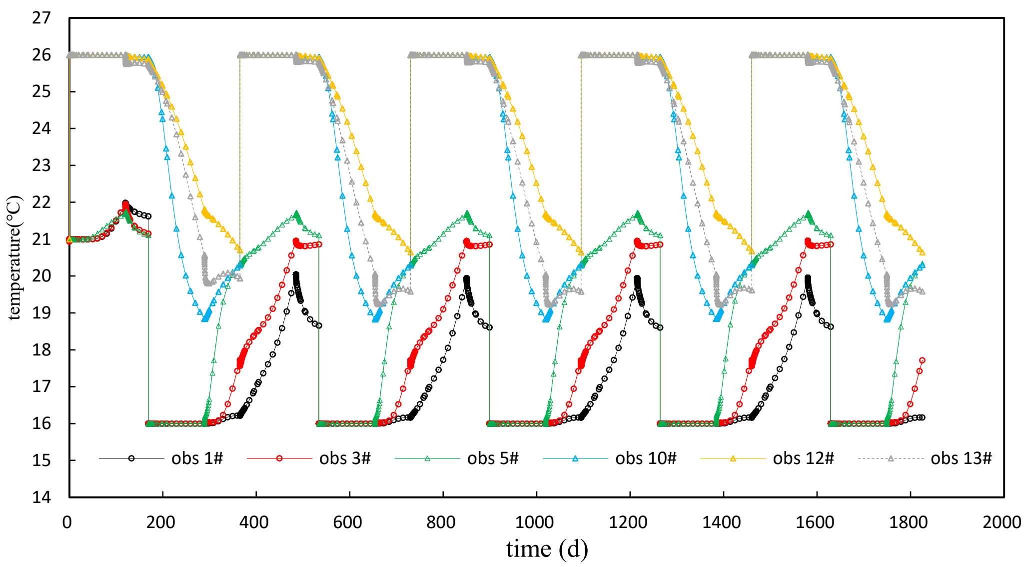

Figure 9. Temperature vs. time for observation wells (F3).

After the first heating period, the temperature of well 5# rises faster than that of wells 1# and 3#; this is because well 5# is mainly affected by the local groundwater. At the beginning of the second cooling period, the initial temperatures of pumping wells 1#, 3#, and 5# are 16.2, 17.7, and 20.3 °C, respectively. During the second cooling period, the temperature of pumping well 5# rises rapidly to 21.1 °C on day 70, with a peak value of 21.7 °C. Although the temperatures of pumping wells 1# and 3# also increase continually, the final temperatures are 20.0 and 20.9 °C, respectively, which are lower than the temperature of local groundwater. At the end of the second heating period, the temperatures of pumping wells 10#, 12#, and 13# reach 18.8, 21.7, and 20.1 °C, respectively.

4.2.3. Evaluation of Water Source Heat Pump Operation Efficiency

The relationship of the operation efficiency coefficient η vs. time for the optimized operation schemes F2 and F3 is shown in Figure 10. On the whole, the parameter of η gradually decreases over time during both the cooling periods and the heating periods.

The mean values of η in the heating periods are higher than those in the cooling periods, and the ranges of η are much wider in the heating periods.

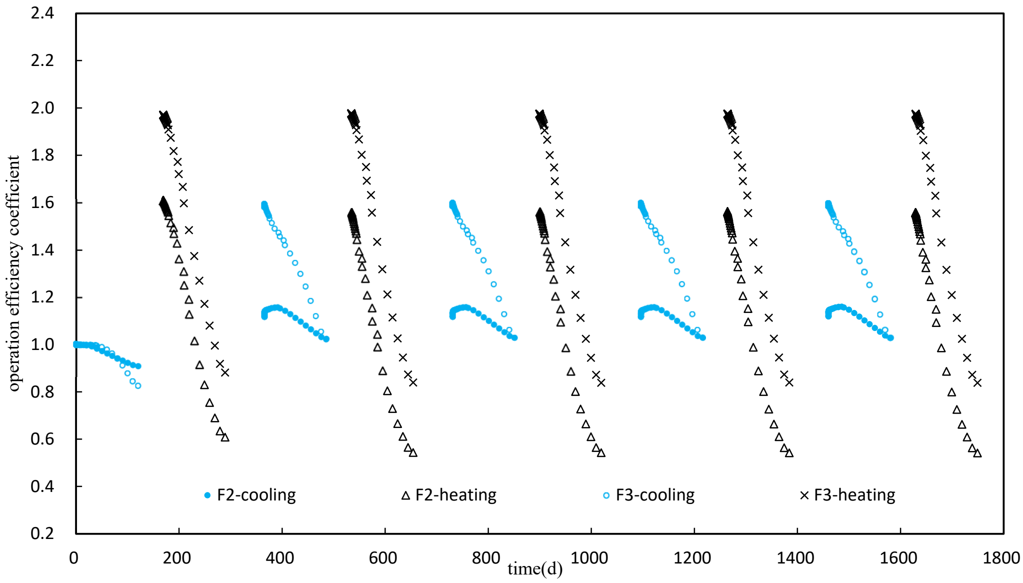

Figure 10. The relationship of operation efficiency coefficient vs. time for the present operation (F2 and F3).

For the operation scheme F2, in the first cooling period, the value of η starts to decrease on day 30, then decreases to 0.91 on day 120. In the first heating period, the value of η continually decreases from 1.61 to 0.61. In the second year, the value of η increases at the beginning of the second cooling period, then decreases from 1.15 on day 30 to 1.02, which shows that the operation efficiency is higher in the second cooling period than in the first. In the second heating period, the value of η goes down from 1.56 to 0.54.

For the operation scheme F3, the value of η continues to decline throughout the entire cooling and heating periods. However, in the second cooling period, the initial value of η is 1.59, which is higher than that during the first cooling. In the second heating period, the initial value of η is 1.98, and at the end of heating, η is still high, with a value of 0.84, which indicates that changing the place of pumping wells and injection wells could provide a much higher temperature for the heating and a lower temperature for the cooling, thereby improving the operation efficiency of the SGE system.

The relationship of η vs. time in both cooling and heating periods of the second year is stable, with an identical and interannual feature for F2 and F3, indicating that the SGE system operated with the same total annual power.

5. Discussion and Conclusions

5.1. Discussion

The operational efficiency of the SGE system can be improved by adjusting the distribution of pumping and injection wells. The phenomenon of heat transport plays an importance role in the operation efficiency of the SGE system, so the operation scheme could be changed to reduce heat transfixion.

In the current operation scheme, the degree of heat transfixion is significant, especially for pumping well 1#, which is located downstream of the SGE. If the location of pumping wells cannot be changed, the injection groundwater, which has a higher temperature in the last cooling period or a lower temperature in the last heating period, cannot be adequately utilized in the heating or cooling periods. The locations of pumping and injection wells of operation schemes F2 and F3 are adjusted. According to Figures 7 and 10, in general, the values of the operation efficiency coefficient η for the optimized schemes of F2 and F3 are higher than those of the current scheme.

According to Formula (7), the practical minable shallow geothermal energy could be analyzed. The linear relationship of the accumulated minable shallow geothermal energy of the three schemes vs. time is shown in Figure 11, i.e., $\Delta E_{pr} = 3535.2t$, correlation coefficient R = 0.99 for F1; $\Delta E_{pr} = 4719.2t$, correlation coefficient R = 0.99 for F2; $\Delta E_{pr} = 5949.9t$, correlation coefficient R = 0.99 for F1. The total accumulated minable shallow geothermal energy for F1, F2, and F3 is 6.33, 8.45, and 10.85 million kwh, respectively, which indicates the higher efficiency of the optimized operation schemes without increasing the operating cost of the SGE system.

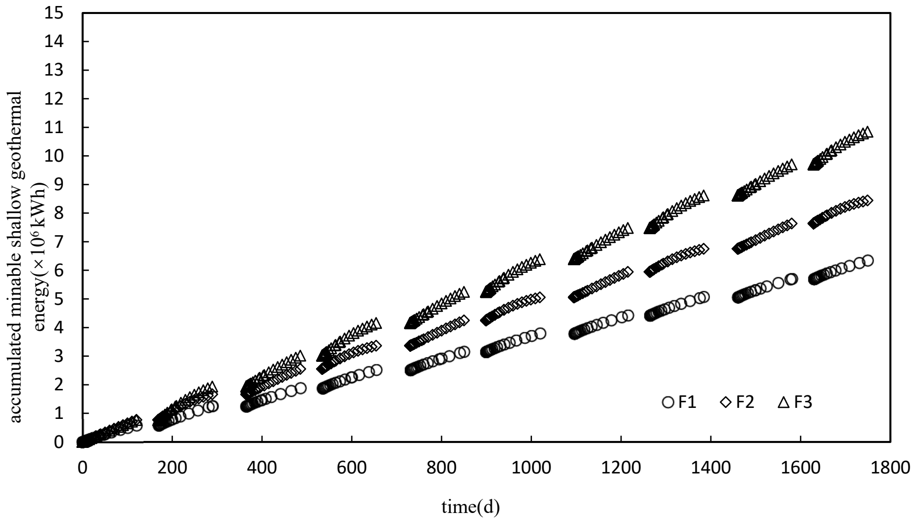

Figure 11. The accumulated minable shallow geothermal energy vs. time for the three operation schemes.

5.2. Conclusions

The phenomenon of heat transfixion occurs in all of the operation schemes, resulting from the distribution of the pumping and injection wells, the local groundwater flow field, and running the models of pumping and injection wells, which reduces the operation efficiency of the SGE system. In order to control the occurrence of heat transfer, it is recommended to adjust the spatial distribution of injection and pumping wells. In cooling periods, the injection well can recharge the higher-temperature water in the aquifer with more thermal energy, which can be utilized in the heating period. In the heating period, some of the injection wells are designed as pumping wells, which reduces the degree of heat transfixion and significantly improves the operation efficiency, by 71.5%. According to the simulation results of the optimized operation schemes, it is suggested that the operation time for each heating or cooling period is reduced to 100 days. As a result, in the future, the phenomenon of heat transfixion may disappear, leading to higher operation efficiency. In fact, the operation efficiency of the SGE system can be affected by many other factors, such as the temperature of the local groundwater, the heat retaining property of pipes, and the efficiency of the heat exchanger collector.

Author Contributions: Introduction, methods, results, discussion, and conclusion, Q.W.; software, Q.W. and X.W.; study area and writing—review and editing, Q.W. and Y.F. All authors have read and agreed to the published version of the manuscript.

Funding: The authors received support from the Fundamental Research Funds for Central Public Welfare Research Institutes (Grant Nos. CKSF2021488/YT, CKSF2023360/YT) and the National Nature Science Foundation of China (Grant Nos. 42072282, 41902260).

Institutional Review Board Statement: Not applicable.

Informed Consent Statement: Not applicable.

Data Availability Statement: The data used to support the findings of this study are included within the article.

Acknowledgments: The authors are grateful for advices for the model setup by Jin Luo, and for the materials about the SGE system by Wang Wanli. Thanks to all members who offered helpful advice for this study.

Conflicts of Interest: The authors declare no conflict of interest.

References

1. Wang, G.L.; Zhang, W.; Lin, W.J.; Liu, F.; Gan, H.; Fu, L. Project progress of survey, evaluation and exploration demonstration of national geothermal resource. *Geol. Surv. China* **2018**, *5*, 1–7.
2. Fan, S.; Lu, Z. Research on the Peak Carbon Dioxide Emission Strategy of Chinese Port Based on Carbon Emission Estimation. *Front. Environ. Sci.* **2022**, *9*, 646. [CrossRef]
3. Haehnlein, S.; Bayer, P.; Blum, P. International legal status of the use of shallow geothermal energy. *Renew. Sustain. Energy Rev.* **2010**, *14*, 2611–2625. [CrossRef]
4. Ahmed, A.A.; Assadi, M.; Kalantar, A.; Sliwa, T.; Sapińska-Śliwa, A. A Critical Review on the Use of Shallow Geothermal Energy Systems for Heating and Cooling Purposes. *Energies* **2022**, *15*, 4281. [CrossRef]
5. Dalla Longa, F.; Nogueira, L.P.; Limberger, J.; van Wees, J.D.; van der Zwaan, B. Scenarios for geothermal energy deployment in Europe. *Energy* **2020**, *206*, 118060. [CrossRef]
6. Wenjing, L.; Qinghua, W.; Guiling, W. Shallow geothermal energy resource potential evaluation and environmental effect in China. *J. Arid Land Resour. Environ.* **2012**, *26*, 57–61.
7. Hakkaki-Fard, A.; Aidoun, Z.; Ouzzane, M. Applying refrigerant mixtures with thermal glide in cold climate air-source heat pumps. *Appl. Therm. Eng.* **2014**, *62*, 714–722. [CrossRef]
8. Sayyaadi, H.; Amlashi, E.H.; Amidpour, M. Multi-objective optimization of a vertical ground source heat pump using evolutionary algorithm. *Energy Convers. Manag.* **2009**, *50*, 2035–2046. [CrossRef]
9. Aquino, A.; Scrucca, F.; Bonamente, E. Sustainability of Shallow Geothermal Energy for Building Air-Conditioning. *Energies* **2021**, *14*, 7058. [CrossRef]
10. Drijver, B.; Willemsen, A. Groundwater as a Heat Source for Geothermal Heat Pumps. *Int. Course Geotherm. Heat Pumps* **1998**, *2*, 156–166.
11. Chang, K.S.; Kim, M.J. Thermal performance evaluation of vertical U-loop ground heat exchanger using in-situ thermal response test. *Renew. Energy* **2016**, *87*, 585–591. [CrossRef]
12. Liu, X.; Xiao, Y.; Inthavong, K.; Tu, J. Experimental and numerical investigation on a new type of heat exchanger in ground source heat pump system. *Energy Effic.* **2015**, *8*, 845–857. [CrossRef]
13. Cui, P.; Yang, H.; Fang, Z. Heat transfer analysis of ground heat exchangers with inclined boreholes. *Appl. Therm. Eng.* **2006**, *26*, 1169–1175. [CrossRef]
14. Najib, A.; Zarrella, A.; Narayanan, V.; Bourne, R.; Harrington, C. Techno-economic parametric analysis of large diameter shallow ground heat exchanger in California climates. *Energy Build.* **2020**, *228*, 110444. [CrossRef]
15. Sivasakthivel, T.; Murugesan, K.; Thomas, H.R. Optimization of operating parameters of ground source heat pump system for space heating and cooling by Taguchi method and utility concept. *Appl. Energy* **2014**, *116*, 76–85. [CrossRef]
16. Koroneos, C.J.; Nanaki, E.A. Nanaki. Environmental impact assessment of a ground source heat pump system in Greece. *Geothermics* **2017**, *65*, 1–9. [CrossRef]
17. Luo, Z.; Wang, Y.; Zhou, S.; Wu, X. Simulation and prediction of conditions for effective development of shallow geothermal energy. *Appl. Therm. Eng.* **2015**, *91*, 370–376. [CrossRef]
18. Dandan, Y.; Zujiang, L.; Yan, W.; Dezhong, Z.; Lianyu, F. Heat balance analysis and countermeasure of groundwater heat pump system of Zhengding in Hebei. *J. Jiangsu Univ. (Nat. Sci. Ed.)* **2015**, *36*, 485–490.
19. Yanzhang, Z.H.O.U.; Zhifang, Z.H.O.U.; Rong, W.U. Simulation study of the stage-characteristics of groundwater thermal transport in aquifer medium for GWHP System. *Hydrogeol. Eng. Geol.* **2011**, *38*, 128–134.
20. Bulté, M.; Duren, T.; Bouhon, O.; Petitclerc, E.; Agniel, M.; Dassargues, A. Numerical Modeling of the Interference of Thermally Unbalanced Aquifer Thermal Energy Storage Systems in Brussels (Belgium). *Energies* **2021**, *14*, 6241. [CrossRef]
21. Russo, S.L.; Gnavi, L.; Roccia, E.; Taddia, G.; Verda, V. Groundwater Heat Pump (GWHP) system modeling and Thermal Affected Zone (TAZ) prediction reliability: Influence of temporal variations in flow discharge and injection temperature. *Geothermics* **2014**, *51*, 103–112. [CrossRef]
22. Lund, J.; Sanner, B.; Rybach, L.; Curtis, R.; Hellström, G. Geothermal(ground–source) heating pumps—A world overview. *GHC Bull.* **2004**, *9*, 1–10.